

## Twirling and Whirling: Viscous Dynamics of Rotating Elastic Filaments

Charles W. Wolgemuth,<sup>1</sup> Thomas R. Powers,<sup>3</sup> and Raymond E. Goldstein<sup>1,2</sup>

<sup>1</sup>Department of Physics, University of Arizona, Tucson, Arizona 85721

<sup>2</sup>Program in Applied Mathematics, University of Arizona, Tucson, Arizona 85721

<sup>3</sup>Division of Engineering and Applied Sciences, Harvard University, Cambridge, Massachusetts 02138  
(Received 30 July 1999)

Motivated by diverse phenomena in cellular biophysics, including bacterial flagellar motion and DNA transcription and replication, we study the overdamped nonlinear dynamics of a rotationally forced filament with twist and bend elasticity. Competition between twist injection, twist diffusion, and writhing instabilities is described by coupled PDEs for twist and bend evolution. Analytical and numerical methods elucidate the twist/bend coupling and reveal two regimes separated by a Hopf bifurcation: (i) diffusion-dominated axial rotation, or *twirling*, and (ii) steady-state crankshafting motion, or *whirling*. The consequences of these phenomena for self-propulsion are investigated, and experimental tests proposed.

PACS numbers: 87.16.-b, 05.45.-a, 46.70.Hg, 47.15.Gf

Dynamics and stability of rotationally forced elastic filaments arise in several important biological settings involving bend and twist elasticity at low Reynolds number. In the context of DNA replication, when two daughter strands are produced from a duplex, it was noted [1] long ago that energy dissipation for rotations about the filament axis is so much smaller than that for transverse motions that axial “speedometer-cable” motions are favored, and are energetically and topologically feasible. During DNA transcription, in which a polymerase protein moves down the double-stranded filament, progressive unwinding of the helix can lead to an accumulation of local twist that may induce “writhing” instabilities of the filament [2]. Energetic and dynamical aspects of these processes are of great current interest [3,4].

At the cellular level, bacteria are propelled through fluids by helical flagella turned by rotary motors in the cell wall [5]. Recent studies [6] have revealed the details of two competing crystal structures assumed by flagellin, the protein building block of flagella, corresponding to helices of opposite chirality. Both local and distributed torques can change the conformation of flagella; during swimming these motors episodically reverse direction [7], and the resultant torques can induce transformations between these states [8], while uniform flow past a pinned flagellum may induce such inversions [9].

To elucidate fundamental processes common to these systems, we consider here the model problem shown in Fig. 1: a slender elastic filament in a fluid of viscosity  $\eta$ , rotated at one end at frequency  $\omega_0$  with the other free. We study competition between three processes: twist injection at the rotated end, twist diffusion, and writhing. Analytical and numerical methods reveal two dynamical regimes of motion: *twirling*, in which the straight but twisted rod rotates about its centerline, and *whirling*, in which the centerline of the rod writhes and crankshaft around the rotation axis in a steady state.

This work is a natural outgrowth of recent studies of forced filaments in the plane [10,11] and dynamic twist-

bend coupling [12–14]. The balance considered between elastic and viscous stresses complements that between elasticity and inertia in the inviscid limit (as in whirling shafts [15,16]), where twist waves propagate [15,17].

An elastic filament is characterized by two geometrical quantities, its radius  $a$ , and contour length  $L$ , and two material quantities, its bending modulus  $A$ , and twist modulus  $C$ . The total elastic energy cost  $\mathcal{E}$  for curvature  $\kappa$  and twist density  $\Omega$  is an integral over arclength  $s$  parametrizing the position  $\mathbf{r}(s, t)$  of the filament centerline [15],

$$\mathcal{E} = \int_0^L ds \left( \frac{A}{2} \kappa^2 + \frac{C}{2} \Omega^2 - \Lambda \right), \quad (1)$$

where the Lagrange multiplier  $\Lambda(s)$  enforces local inextensibility,  $(\mathbf{r}_t)_s \cdot \mathbf{r}_s = 0$ . Thus arise two dimensionless ratios:  $\Gamma \equiv C/A$  and the aspect ratio  $a/L$ . At zero Reynolds number, elastic forces per length  $\mathbf{f} \equiv -\delta\mathcal{E}/\delta\mathbf{r}$  [18] balance the viscous drag from slender-body hydrodynamics [19]:

$$\zeta_{\parallel} \hat{\mathbf{t}} \cdot \mathbf{r}_t + \zeta_{\perp} (\mathbf{I} - \hat{\mathbf{t}} \hat{\mathbf{t}}) \cdot \mathbf{r}_t = \mathbf{f}, \quad (2)$$

where  $\hat{\mathbf{t}} = \mathbf{r}_s$  is the unit tangent, and the transverse and longitudinal drag coefficients are  $\zeta_{\perp} \approx 2\zeta_{\parallel} \approx 4\pi\eta/[\ln(L/2a) + c]$ , with  $c$  a constant of order

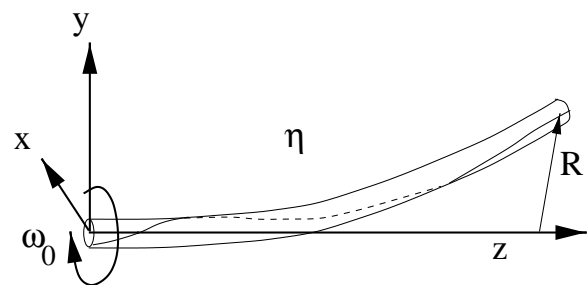


FIG. 1. An elastic filament, rotated about  $z$  at the left end, surrounded by a fluid of viscosity  $\eta$ .

unity [19]. Likewise, the axial elastic torque per unit length  $m = C\Omega_s$  [14,15] balances the local rotational drag:  $m = \zeta_r \omega$ , where  $\omega(s, t)$  is the local rotational velocity about  $\hat{\mathbf{t}}$  and  $\zeta_r \approx 4\pi\eta a^2$  [19]. We also define  $\epsilon^2 \equiv \zeta_r/(\zeta_\perp L^2)$ , so that  $\epsilon \sim (a/L)$ , apart from logarithmic corrections.

The dynamics are closed by a geometric constraint,

$$\Omega_t = \omega_s + (-\Omega \mathbf{r}_s + \mathbf{r}_s \times \mathbf{r}_{ss}) \cdot [\mathbf{r}_t]_s, \quad (3)$$

which shows how twist changes due to differential rates of angular rotation, stretching (e.g., extension of a straight, twisted rod decreases  $\Omega$ ), and out-of-plane bending motions (writhing) [12–14]. The constraint (3) is a conservation law for twist density  $\Omega$ , with twist current  $-\omega$ , and with the stretching and writhing terms acting as sinks or sources. The velocities  $\omega$  and  $\mathbf{r}_t$  enter (3) through their space derivatives, since rigid motions cannot change  $\Omega$ . With the local torque balance  $\zeta_r \omega = C\Omega_s$  and assuming inextensibility we obtain

$$\Omega_t = \frac{C}{\zeta_r} \Omega_{ss} + \frac{1}{\zeta_\perp} \mathbf{r}_s \times \mathbf{r}_{ss} \cdot \mathbf{f}_s. \quad (4)$$

The second term of (4) is nonzero [20] when the filament is both out of elastic equilibrium ( $\mathbf{f} \neq 0$ ) and either non-planar (with torsion  $\tau \neq 0$ ) or twisted ( $\Omega \neq 0$ ), and then acts as a sink or source of twist.

For boundary conditions, we assume that the forced end  $[\mathbf{r}(0) = 0]$  of the rod is clamped  $[\mathbf{r}_s(0) = \hat{\mathbf{z}}]$  and the free end experiences no force or torque  $[\mathbf{r}_{ss}(L) = \mathbf{r}_{sss}(L) = 0; \Omega(L) = 0]$ . Local torque balance sets  $\Omega_s(0) = \zeta_r \omega_0/C$ .

Before solving these partial differential equations (PDEs) numerically, we use dimensional analysis to understand the main features of the motion. We focus on small-amplitude bend and twist deformations of a straight filament (thus ignoring  $\zeta_\parallel$ ). Of the seven parameters ( $A, C, L, a, \zeta_r, \zeta_\perp, \omega_0$ ), four remain after introducing  $\Gamma$  and  $\epsilon$  and noting that  $a$  appears only through  $\zeta_r$ , so suitable rescalings of length, time, and  $\Omega$  leave only one control parameter. This can be chosen proportional to the rotation frequency  $\omega_0$ .

For low turning rates  $\omega_0$ , the filament remains straight, with twist diffusion and injection balancing. The twist density at the clamped end follows from a balance of viscous and elastic twisting torques,  $\zeta_r \omega_0 L \sim C\Omega(0)$ . Instability occurs when the twist torque  $C\Omega$  is comparable to the filament buckling torque  $A/L$  [15]. At this point, the balance of viscous and twist torques implies

$$\omega_c \sim \frac{A}{\zeta_r L^2} \sim \left(\frac{a}{L}\right)^2 \frac{E}{\eta} \sim \frac{k_B T}{\zeta_r L_p} \left(\frac{L_p}{L}\right)^2, \quad (5)$$

where the second and third results follow from the relations  $A = (\pi/4)a^4 E$  between the bending modulus and the Young's modulus  $E$  [15] and  $A = k_B T L_p$ , with  $L_p$  the persistence length. Interestingly,  $\omega_c$  is independent of the twist modulus  $C$ , and since the twist density scales with the drag,  $\omega_c$  varies inversely with  $\zeta_r$ .

The result (5) is central, because naive dimensional analysis predicts  $\omega_c \sim E/\eta$ . With  $E \sim 10^7$  dyn/cm<sup>2</sup> and  $\eta \sim 0.01$  P as for rubber in water,  $\omega_c$  would be enormous if not for the prefactor  $(a/L)^2$ . Since  $a/L$  is reasonably  $10^{-3}$ , we find  $\omega_c \sim 10^3$  s<sup>-1</sup>, similar to flagella rotation rates [5] and achievable in the laboratory. The rightmost form in (5) readily shows the frequency scales for systems of varying length and stiffness. Consider the elastic filaments DNA ( $L_p \sim 5 \times 10^{-6}$  cm,  $a \sim 10^{-7}$  cm), microtubules ( $L_p \sim 0.5$  cm,  $a \sim 10^{-6}$  cm), and bacterial filaments ( $L_p \sim 25$  cm,  $a \sim 3 \times 10^{-5}$  cm) [21]. The frequencies  $k_B T/\zeta_r L_p$  are then  $8 \times 10^6$ , 0.8, and  $1.3 \times 10^{-5}$  s<sup>-1</sup>, respectively. Thus, for the instability to appear at, say,  $10^3$  s<sup>-1</sup> requires a minimum ratio  $L/L_p$  of 90, 0.03, and  $10^{-4}$ . A strand of DNA with  $L/L_p \sim 10^2$  is clearly not straight in isolation, so this instability would be hard to realize in DNA, but the stiffer examples of microtubules and bacterial filaments are indeed candidates.

Linearizing (2) and (4) about a straight filament along  $\hat{\mathbf{z}}$ , with  $\mathbf{r} \approx s\hat{\mathbf{z}} + \mathbf{r}_\perp$ , we see that twist diffuses with diffusion constant  $C/\zeta_r$ , while the backbone obeys a ‘‘hyperdiffusion’’ equation  $\zeta_\perp \mathbf{r}_{\perp t} = -A\mathbf{r}_{\perp ssss} + C\hat{\mathbf{z}} \times (\Omega \mathbf{r}_{\perp ss})_s$ . For crankshafting motions, we set  $\mathbf{r}_{\perp t} = \chi \hat{\mathbf{z}} \times \mathbf{r}_\perp$ . Thus we find two characteristic lengths [10],

$$\ell_\perp(\chi) = (A/\zeta_\perp \chi)^{1/4}, \quad \ell_r(\omega_0) = (C/\zeta_r \omega_0)^{1/2}. \quad (6)$$

These are analogous to the penetration depth in the familiar theory of oscillations in a viscous fluid [22]. The primary instability is given by  $\ell_r(\omega) \sim L$ .

The crankshafting frequency  $\chi$  for whirling can be estimated by assuming that the transverse drag, force per length,  $\zeta_\perp \chi |\mathbf{r}_\perp|$ , is roughly equal to the elastic force per length,  $A |\mathbf{r}_{\perp 4s}| \sim A |\mathbf{r}_\perp|/L^4$ . Thus  $\chi \sim A/\zeta_\perp L^4 \sim (a/L)^2 \omega_c$  ( $C \approx A$  for typical materials [15]), and  $\ell_\perp(\chi) \sim \ell_r(\omega_c) \sim L$  at the transition. The whirling rod of course does not undergo simple rigid body rotation; the speedometer-cable rotational motion is faster than the backbone crankshafting motion by a factor of  $(L/a)^2$ . This steady-state shape is possible because diffusion can homogenize the twist as fast as backbone motion relieves it. We describe this process quantitatively by integrating (3) along the rod for inextensible, steady-state ( $\Omega_t = 0$ ) crankshafting. The difference  $\Delta\omega$  in rotational velocities about the local tangents at  $s = L$  and  $s = 0$  is

$$-\Delta\omega = \chi[1 - \hat{\mathbf{z}} \cdot \hat{\mathbf{t}}(L)]. \quad (7)$$

Equivalently,  $\Delta\omega$  is the injected twist current minus the twist current leaving the free end. Thus, writhing acts as a twist sink in steady-state crankshafting motion when the rod's free end is not aligned with the  $z$  axis.

When the twist diffusion time,  $\zeta_r L^2/C$ , is longer than the bending time,  $\chi^{-1}$ , buckling can relieve twist faster than it is replenished by diffusion, and steady-state crankshafting would likely be unstable. One possible new behavior would consist of repeated sequences of transient whirling followed by quiescence as twist builds

up anew. Scaling arguments yield a critical frequency of  $\omega_0 \sim E/\eta$ , a factor of  $\epsilon^{-2}$  higher than the rate at the onset of the first instability, and thus unreachable for typical materials.

The bend relaxation time suggests the rescaling,

$$\tilde{t} \equiv (A/\zeta_{\perp} L^4). \quad (8)$$

A natural pair of further rescalings of (4) is  $\tilde{s} = s/L$  and  $\tilde{\Omega} = \Omega L$ . If we parametrize the filament centerline (Fig. 1) as  $\mathbf{r}(s, t) = [X(s, t), Y(s, t), s - \delta(s, t)]$ , introduce the complex transverse displacement  $\xi = (X + iY)/L$ , and expand the dynamics up to third order in  $\xi$  (immediately dropping the tildes), we obtain

$$\begin{aligned} \xi_t = & -\xi_{4s} - (\Lambda \xi_s)_s + i\Gamma\{\Omega[\xi_{ss}(1 - \delta_s) + \delta_{ss}\xi_s]\}_s \\ & - \left[ \frac{1}{2}(\xi_{4s}^* \xi_s + \xi_{4s} \xi_s^*) + \Lambda_s \right] \xi_s, \quad (9) \\ \Omega_t = & \frac{\Gamma}{\epsilon^2} \Omega_{ss} - \text{Im}(\xi_{5s}^* \xi_{ss}) + \Gamma \text{Re}[(\Omega \xi_{ss}^*)_{ss} \xi_{ss}] \end{aligned}$$

where the inextensibility constraint  $(1 - \zeta_{\parallel}/\zeta_{\perp})(\mathbf{r}_{ss} \cdot \mathbf{f}) + (\mathbf{r}_s \cdot \mathbf{f}_s) \approx \frac{1}{2}(\mathbf{r}_{ss} \cdot \mathbf{f}) + (\mathbf{r}_s \cdot \mathbf{f}_s) = 0$  is expanded to set  $\Lambda$  as

$$\left( \Lambda - \frac{3}{2} |\xi_{ss}|^2 \right)_{ss} = \frac{1}{2} [\text{Re}(\xi_{4s} \xi_{ss}^*) + i\Gamma \Omega \text{Im}(\xi_{3s} \xi_{ss}^*)].$$

This constraint also fixes  $\delta_s \approx \frac{1}{2} |\xi_s|^2$ . As anticipated, apart from material properties  $\Gamma$  and  $\epsilon$ , the coupled twist/bend dynamics are governed by a single control parameter  $\omega_0$ , which appears only in the (rescaled) boundary condition,  $\Omega_s(0) = \epsilon^2 \omega_0/\Gamma = \alpha$ . The PDEs (9) are like those of excitable media [23], with a separation of time scales derived from the aspect ratio  $\epsilon$ . For the usual case  $\epsilon \ll 1$ , twist is the fast variable and bends are slow.

*Linearized dynamics.*—The twist profile in the straight filament ( $\xi = 0$ ) satisfies  $\Omega_t = (\Gamma/\epsilon^2)\Omega_{ss}$ . After transients die out, the steady-state profile is linear in  $s$  [3],  $\Omega = (\zeta_r \omega_0/C)(s - L)$ . Using this in the linearized filament evolution and taking  $\xi(s, t) = \xi(s) \exp(i\chi t)$ , a rigidly rotating, neutrally stable shape, we obtain

$$\chi \xi = i\xi_{4s} + \Gamma \alpha [(s - 1)\xi_{ss}]_s. \quad (10)$$

Numerical solution [24] of (10) yields a critical value  $\alpha_c \approx 8.9/\Gamma$  [confirming dimensional analysis of Eq. (8)], below which the rod is straight and executes only axial rotation (“twirling”), and above which the rod buckles and rotates (“whirls”) at a frequency which for  $\alpha \approx \alpha_c$  is  $\chi \approx 2.32\Gamma\alpha$ . This motion is the dynamical equivalent of the static writhing instability of a twisted filament [15]. Inserting all numerical factors, the critical frequency and rotation rate (at onset) are

$$\omega_c \approx 0.563 \left( \frac{a}{L} \right)^2 \frac{E}{\eta}, \quad \chi_c \approx 20.9 \left( \frac{a}{L} \right)^2 \omega_c. \quad (11)$$

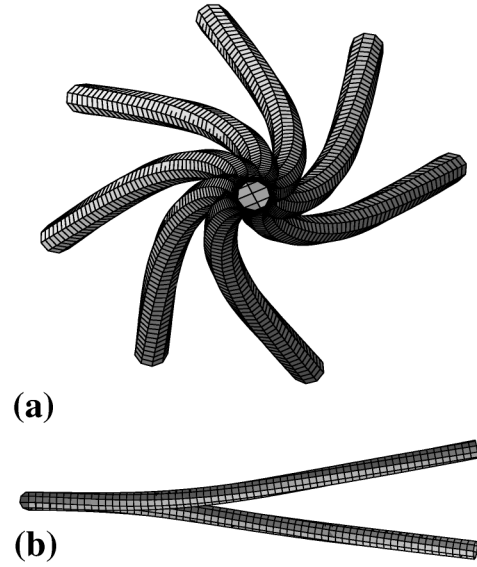


FIG. 2. (a) Stroboscopic montage of the “whirling” filament, viewed from along the  $z$  axis, as it rotates clockwise; (b) side view at 2 times, drawn to a different scale.

*Weakly nonlinear theory.*—Numerical solution of (9) with a pseudospectral method [14,25] shows that there is indeed a steady state beyond the bifurcation. As  $\alpha - \alpha_c$  increases, the shape becomes more helical. The free end of the whirling filament experiences more drag than points closer to the driven end and thus lags behind (Fig. 2). Since  $\Omega$  depends quadratically on the backbone shape [see

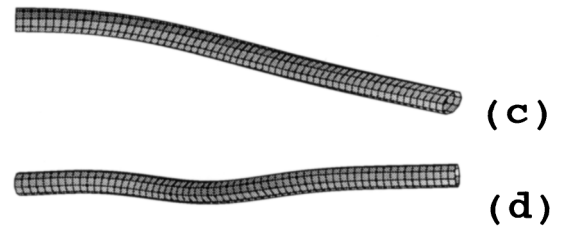
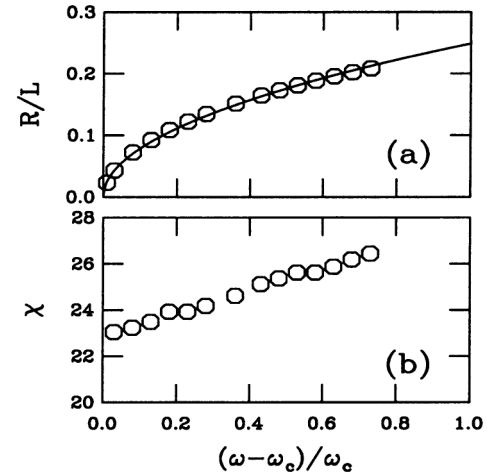


FIG. 3. (a) Amplitude  $R$  (with a square root fit), and (b) crankshafting frequency of filament tip motion as a function of frequency offset from primary instability. (c),(d) filament shapes for  $(\omega_0 - \omega_c)/\omega_c = 0.27$  and  $3.52$ , respectively, with  $\Gamma = 1$ .

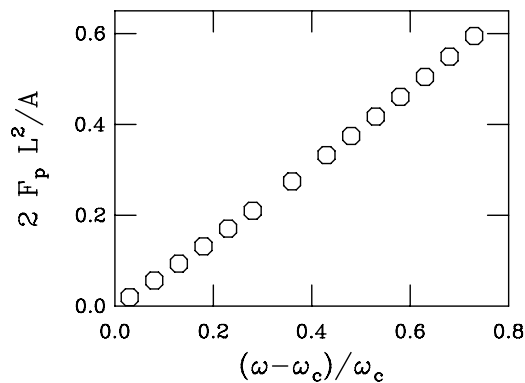


FIG. 4. Propulsive force generated by steady-state whirling motions, as a function of driving frequency.

Eq. (3)], near  $\omega_c$ , where  $\xi$  is small, the twist density remains nearly linear in  $s$ . Numerical studies show that the free end traces out a circle with radius  $R \sim (\omega_0 - \omega_c)^{1/2}$ : a supercritical Hopf bifurcation [23]. This can be understood from (7) and dimensional arguments for the displacement;  $[1 - \hat{\mathbf{z}} \cdot \hat{\mathbf{t}}(L)] \approx (R/L)^2$ , so that  $\omega(0) - \omega(L) \sim \chi(R/L)^2$ . The twist that can be relieved by diffusion is limited, so that  $\omega(L) \approx \omega_c$ . From the linear dynamics,  $\chi \sim \omega_c$ , leading to  $R \sim (\omega_0 - \omega_c)^{1/2}$ .

*Swimming.*—Chirality of the whirling filament breaks time-reversal invariance of the motion, thereby allowing [26] a net propulsive force  $F_p$  along  $\hat{\mathbf{z}}$  to be generated. The elastic force density is a total derivative, so the total force is expressible in terms of the filament properties at its ends. For the clamped/free boundary conditions used here,  $F_p = -\mathbf{r}_{3s}(0) \cdot \hat{\mathbf{z}} - \Lambda(0) = \mathbf{r}_{ss}(0) \cdot \mathbf{r}_{ss}(0) - \Lambda(0)$ . As shown in Fig. 4,  $F_p$  rises linearly from zero near the bifurcation, as it is quadratic in the transverse displacement, which in turn has the supercritical form shown in Fig. 3(a). While we know of no organism that utilizes this precise mechanism for self-propulsion, there is evidence [27] for self-propulsion associated with twist-induced whirling in growing bacterial macrofibers constrained at one end.

The possibility of observing instabilities driven by twist accumulation along a filament hinges upon a balance of material properties, fluid viscosity, and adequate forcing. Flow- and rotation-induced bacterial flagellar conformational transitions [7–9] provide proof-of-principle that this balance can be achieved *in vivo*. Like flagella, fibers of *B. subtilis* cells have adequate material properties (e.g., Young's modulus [21]) and aspect ratio to display instabilities such as those described here. More complex phenomena are associated with instabilities of rotating helical flagella, as described elsewhere [28].

We thank P. Nelson and C. Wiggins for discussions motivating this work, and D. Coombs, A. Goriely, G. Huber, J.O. Kessler, S. Koehler, H.A. Stone, and especially N.H. Mendelson and J.E. Sarlls for ongoing collaborations. This work was supported by NSF Grant No. DMR9812526 (REG); T.R.P. thanks H. Stone for

support through the Harvard MRSEC and the Army Research Office Grant No. DAA655-97-1-014.

- [1] C. Levinthal and H.R. Crane, Proc. Natl. Acad. Sci. **42**, 436 (1956).
- [2] L.F. Liu and J.C. Wang, Proc. Natl. Acad. Sci. U.S.A. **84**, 7024 (1987).
- [3] J.F. Marko, Phys. Rev. E **57**, 2134 (1998).
- [4] P. Nelson, Proc. Natl. Acad. Sci. U.S.A. **96**, 14342 (1999).
- [5] For a review, see K. Namba and F. Vonderviszt, Q. Rev. Biophys. **30**, 1 (1997).
- [6] I. Yamashita *et al.*, Nature (London) **5**, 125 (1998); D.L. Caspar, *ibid.* **5**, 92 (1998), and references therein.
- [7] H.C. Berg and R.A. Anderson, Nature (London) **245**, 380 (1973).
- [8] R.M. Macnab and M.K. Ornston, J. Mol. Biol. **112**, 1 (1977).
- [9] H. Hotani, J. Mol. Biol. **156**, 791 (1982).
- [10] C.H. Wiggins, D. Riveline, R.E. Goldstein, and A. Ott, Biophys. J. **74**, 1043 (1998).
- [11] S. Camalet, F. Jülicher, and J. Prost, Phys. Rev. Lett. **82**, 1590 (1999).
- [12] I. Klapper and M. Tabor, J. Phys. A **27**, 4919 (1994); I. Klapper, J. Comput. Phys. **125**, 325 (1996).
- [13] R.D. Kamien, Eur. Phys. J. B **1**, 1 (1998).
- [14] R.E. Goldstein, T.R. Powers, and C.H. Wiggins, Phys. Rev. Lett. **80**, 5232 (1998).
- [15] A.E.H. Love, *A Treatise on the Mathematical Theory of Elasticity* (Dover Publications, New York, 1944), 4th ed.
- [16] S.S. Antman, Proc. R. Soc. Edinb. A, Math. (UK) **85**, 59 (1980).
- [17] A. Goriely and M. Tabor, Physica (Amsterdam) **105D**, 20 (1997); **105D**, 44 (1997); Proc. R. Soc. London A, Math. **453**, 2583 (1997); **454**, 3183 (1998).
- [18]  $\mathbf{f} = -A\mathbf{r}_{4s} + C[\Omega(\mathbf{r}_s \times \mathbf{r}_{ss})]_s - (\Lambda\mathbf{r}_s)_s$ ; see [15,14]. Note that  $\Lambda$  has been shifted to absorb tangential components of the elastic force  $\int_0^s ds \mathbf{f}$  on a cross section.
- [19] J. Keller and S. Rubinow, J. Fluid Mech. **44**, 705 (1976).
- [20] The writhe-tracking term is  $\mathbf{r}_s \times \mathbf{r}_{ss} \cdot (\mathbf{f}_\perp)_s = -A[3\kappa(\kappa_s\tau)_s + \kappa^2(\tau_{ss} - \tau^3 - \kappa^2\tau)] + C[\kappa(\Omega\kappa)_{ss} - \Omega\kappa^2\tau^2] + \Lambda\kappa^2\tau$ , where  $\tau$  is the (Frenet-Serret) torsion.
- [21] J.J. Thwaites and N.H. Mendelson, Int. J. Biol. Macromol. **11**, 201 (1989).
- [22] G.G. Stokes, Trans. Cambridge Philos. Soc. **9**, 8 (1851).
- [23] M.C. Cross and P.C. Hohenberg, Rev. Mod. Phys. **65**, 851 (1993).
- [24] W.H. Press, W.T. Vetterling, S.A. Teukolsky, and B.P. Flannery, *Numerical Recipes in C* (Cambridge University Press, Cambridge, England, 1992), Chap. X, 2nd ed.
- [25] R.E. Goldstein, D.J. Muraki, and D.M. Petrich, Phys. Rev. E **53**, 3933 (1996).
- [26] G.I. Taylor, Proc. R. Soc. London A **211**, 225 (1952); E.M. Purcell, Am. J. Phys. **45**, 3 (1977).
- [27] N.H. Mendelson, J.E. Sarlls, C.W. Wolgemuth, and R.E. Goldstein, following Letter, Phys. Rev. Lett. **84**, 1627 (2000).
- [28] D. Coombs, G. Huber, R.E. Goldstein, and J.O. Kessler (to be published).